ATP stimulates pannexin 1 internalization to endosomal compartments

Andrew K.J. Boyce, Michelle S. Kim, Leigh E. Wicki-Stordeur, and Leigh Anne Swayne

September 2015

ATP stimulates Pannexin 1 internalization to endosomal compartments

Andrew K. J. Boyce[*], Michelle S. Kim[*], Leigh E. Wicki-Stordeur[*], Leigh Anne Swayne[*§1]

[*]Division of Medical Sciences and Island Medical Program, University of Victoria, Victoria V8P 5C2 Canada

[§]Department of Cellular and Physiological Sciences, University of British Columbia, Vancouver V6T 1Z3, Canada

([1])To whom correspondence should be addressed: Leigh Anne Swayne, Division of Medical Sciences, 3800 Finnerty Rd, Victoria, BC, CANADA, Tel.: (250) 217-2488; Fax (250) 472-5505; E-mail: lswayne@uvic.ca

ABSTRACT

The ubiquitous pannexin 1 (Panx1) ion- and metabolite-permeable channel mediates the release of ATP, a potent signalling molecule. Here we present striking evidence that ATP, in turn, stimulates internalization of Panx1 to intracellular membranes. These findings hold important implications for understanding the regulation of Panx1 when extracellular ATP is elevated. In the nervous system this includes phenomena such as synaptic plasticity, pain, precursor cell development and stroke; outside of the nervous system this includes things like skeletal and smooth muscle activity and inflammation. Within 15 min, ATP led to significant Panx1—EGFP internalization. In a series of experiments, we determined that hydrolyzable ATP is the most potent stimulator of Panx1 internalization. We identified two possible mechanisms for Panx1 internalization, including activation of ionotropic purinergic (P2X) receptors, and involvement of a putative ATP-sensitive residue in the first extracellular loop of Panx1 (W74). Internalization was cholesterol-dependent, but clathrin, caveolin and dynamin independent. Detailed analysis of Panx1 at specific endosome sub-compartments confirmed that Panx1 is expressed in endosome membranes of the classical degradation pathway under basal conditions, and that elevation of ATP levels diverts a subpopulation to recycling endosomes. This is the first report detailing endosome localization of Panx1 under basal conditions and the potential for ATP regulation of its surface expression. Given the ubiquitous expression profile of Panx1 and the importance of ATP signalling, these findings are of critical importance for understanding the role of Panx1 in health and disease.

Summary: ATP stimulates internalization of Panx1. This novel finding raises important considerations with regards to Panx1 surface stability in diverse scenarios in which ATP can be rapidly elevated in the extracellular space.

Running title: *ATP stimulates pannexin 1 internalization*

Keywords: pannexin 1 / pannexin1 / ATP / endocytosis / trafficking / endosomes

INTRODUCTION

Six individual pannexin 1 (Panx1) proteins come together to form channels that facilitate the regulated passage of Ca^{2+} and small molecules across the plasma membrane in cells throughout the body [1]. Panx1 channels are perhaps best known for their association with ATP release from cells and can be opened by several stimuli including mechanical stretch and depolarization of the plasma membrane. ATP, in turn, is a key signalling molecule that acts through various purinergic receptors to modulate a number of important signalling events.

The ubiquitously expressed Panx1 is particularly enriched in the nervous system in developing [2, 3] and mature neurons [4, 5], and astrocytes [6, 7]. There is a growing body of evidence that Panx1 plays key roles in regulating synaptic plasticity [8, 9] and neural cell responses to oxygen and glucose deprivation [10, 11]; recently reviewed in [12] and [13]. The factors regulating Panx1 surface expression in neural cells and therefore its influence on synaptic plasticity and neurobiology are poorly understood.

In the course of our studies on Panx1 in neural precursor cells and neurons, we observed a sizeable, stable sub-population of Panx1 on intracellular membranes, consistent with reports from several other groups studying both neural and non-neural cell types [14-17]. Whether this population resulted from diversion from the secretory pathway or internalization (retrograde trafficking) of mature Panx1 from the plasma membrane was unknown. We reasoned that stable intracellular expression resulting from retrograde Panx1 trafficking would require a stimulus that is episodically released from cells. ATP fits this criterion: it is constitutively released in episodic bursts from many types of neural cells [18, 19]. Here we tested the prediction that elevated extracellular ATP stimulates Panx1 internalization.

METHODS

Cell Culture - Mouse Neuro2a (N2a) neuroblastoma cells (procured from the A.T.C.C.) were cultured in Dulbecco's modified Eagle's medium (DMEM)/F12 supplemented with 10% FBS, 100 units/mL penicillin, and 100 μg/mL streptomycin (all obtained from Gibco/Life Technologies). Human Embryonic Kidney (HEK)293T cells (procured from the A.T.C.C.) were cultured in DMEM supplemented with 10% FBS, 100 units/mL penicillin, and 100 μg/mL streptomycin. Where indicated, N2a and HEK293T cells were transfected using jetPEI reagent (Polyplus transfection/VWR) according to the manufacturer's protocol.

Plasmids - A mutant Panx1—W74A—EGFP plasmid was created by site-directed mutagenesis of the Panx1—EGFP plasmid [20] with the following primers (forward: 5'-CGAGTTCTTTCTCCGCGCGACAGGCTGCCTTTG-3'; reverse: 5'CAAAGGCAGCCTGTCGCGCGGAGAAAGAACTCG-3') using the QuikChange II site-directed mutagenesis kit following manufacturer's protocols (Agilent Technologies) and confirmed by sequencing (Eurofins MWG Operon). Where indicated, N2a cells stably expressing equivalent levels of Panx1—EGFP or Panx1—W74A—EGFP were maintained in DMEM/F12 containing 10% FBS, and 100 units/mL penicillin, 100 μg/mL streptomycin, and 400 μg/mL geneticin 418 (all obtained from Gibco/Life Technologies).

Antibodies - Primary antibodies used were anti-GFP (1:500**,** Roche Applied Science), anti-β-actin (1:160,000; Sigma-Aldrich) anti-early endosome antigen 1 (EEA1; 1:200, Cell Signaling Technology Inc.), anti-lysosomal-associated membrane protein 1 (Lamp1; 1:200), anti-caveolin-1 (Cav-1; 1:100, Novus Biologicals LLC), anti-clathrin heavy chain (1:50; Novus

Biologicals LLC), anti-Ras-related protein Rab14 (Rab14; 1:400, Abcam Inc.), anti-Rab4 (1:200, BD Biosciences), anti-mannose-6-phosphate receptor (M6PR; 1:100, Abcam Inc.), anti-Rab7 (1:200, Abcam Inc.), anti-Rab11 (1: 50, Santa Cruz Biotechnology) and anti-giantin (1: 500, Lifespan Biosciences Inc.). The Panx1 primary antibody used was anti-Panx1 extracellular loops 2 (EL2; 1:200 [21]). Secondary antibodies included horseradish peroxidase (HRP)-conjugated AffiniPure donkey anti-rabbit IgG and HRP-conjugated AffiniPure donkey anti-mouse IgG (both at 1:4000; Jackson ImmunoResearch), Alexa Fluor® 647-conjugated AffiniPure donkey anti-rabbit IgG (1:600; Jackson ImmunoResearch), Alexa Fluor® 568 donkey anti-mouse IgG and Alexa Fluor® 568 donkey anti-rabbit IgG (both at 1:600; Life Technologies).

Live and Fixed Cell Imaging: Cells were treated in media containing 20 μg/mL cycloheximide (CHX; Sigma-Aldrich) for 8 h prior to experimental treatments. Confocal imaging was performed with a Leica TCS SP8 confocal microscope and analysis was performed with Leica Application Suite software (version 3.1.3). All imaging and quantification were performed double-blinded to treatment conditions. Comparisons were made under identical conditions. Confocal micrographs displayed as representative images were adjusted for contrast uniformly using Adobe Photoshop for display purposes only; no contrast adjustments were made prior to analysis. Stimulated Emission Depletion (STED) confocal microscopy [22] was performed on a Leica TCS SP8 STED confocal microscope and deconvolution was performed using the Huygens Professional Deconvolution software (Suite 15.05) [23].

Live Cell Panx1 Tracking - N2a cells stably expressing Panx1—EGFP were plated on 100 μg/mL poly-D-lysine (PDL)-coated eight-well chambered coverglass (Nunc LabTek/ ThermoScientific) and maintained at a temperature of 37 °C and 5 % CO_2. Tetramethylrhodamine (TRITC)-conjugated wheat germ agglutinin (WGA; 1 μg/mL; Life Technologies) was added 5 min prior to imaging. ATP (100 μM, 200 μM, 500 μM; Sigma-Aldrich) or vehicle control (water) was added to individual wells and images were collected at 1-min intervals for 30 min using a 20x (0.7 numerical aperture (NA)) objective. Quantification of Panx1—EGFP fluorescence intensity to describe 'intracellular Panx1' was performed at time zero and each 5-min interval thereafter, as follows: a polygonal trace was drawn 1 μm inside of the peak WGA intensity at the cell periphery and the encapsulated average Panx1—EGFP fluorescence intensity per pixel was computed (Figure 1). Data were normalized to values obtained at time zero. $N \geq 25$ cells were analysed per experimental condition per biological replicate. Only cells that were stable in the z-axis for the entire imaging window were counted.

Fixed Cell Panx1 Localization - N2a cells stably expressing Panx1—EGFP were plated on PDL-coated coverslips in 24 well plates. Cells were cultured and pre-treated briefly with CHX as described above in the live cell confocal experiments. Where indicated, other stimuli or drugs were added to the culture media, in the presence of CHX, including: 30 mM potassium chloride (K^+), 10 μM Ca^{2+} ionophore A23187, chemical oxygen glucose deprivation (OGD; 100 μM potassium cyanide and 1 μg/mL oligomycin), 100 μM or 500 μM 2'(3')-O-(4-benzoylbenzoyl) adenosine 5'-triphosphate triethylammonium salt (BzATP), 500 μM UTP Tris salt, 500 μM adenosine-5'-(β-thio)-diphosphate trilithium salt (ADPβS; all obtained from Sigma-Aldrich) or 500 μM adenosine-5'-(γ-thio)-triphosphate tetralithium salt (ATPγS; Tocris Bioscience). For the P2X7 or endocytosis inhibitor experiments, cells were pre-treated for 1 h prior to 500 μM ATP or control treatment with 100 μM A438079 (Tocris Bioscience), or 10 μg/mL chlorpromazine (CLPZ), 1 μg/mL filipin III (Fil III), 10 mM methyl-β-cyclodextrin (MβCD) or vehicle control (equal volume of DMSO; all endocytosis inhibitors obtained from Sigma-Aldrich) respectively. Following ATP/control treatment, cells were fixed with 4%

paraformaldehyde in PBS for 10 min. Coverslips were then incubated with primary antibodies in antibody buffer (3% BSA, 0.3% Triton-X-100 in PBS) overnight at 4°C, washed and incubated with corresponding fluorophore-conjugated secondary antibody and Hoechst 33342 nuclear counterstain in antibody buffer for 1 h at room temperature, then washed and mounted in VectaShield (Vector Labs). $N \geq 50$ cells were analysed per experimental condition per biological replicate. Confocal images were obtained at 4x optical zoom in 1024 x 1024 format with a pixel area of 71 nm^2 at room temperature using a 40x (1.3 NA) oil immersion objective as confocal z-stacks and quantification was performed in the confocal plane displaying the largest central plane of the nuclei in the region of interest. Intracellular Panx1 was quantified as described above (and in Figure 1) and normalized to values obtained for vehicle-treated controls. STED imaging of selected regions of interest was performed to support localization to specific compartments obtained with conventional confocal microscopy with enhanced resolution. STED images were obtained with a pixel area of 39 nm^2 using a 100X (1.4 NA) oil immersion STED white objective. This allowed for a theoretical maximum resolution of approximately 80 nm prior to deconvolution. Deconvolution removes aberrations and increases the contrast of the image allowing for an increase in resolution by a factor of 1.5-2 [23]. Analysis of background speckular structures (reflecting single antibody molecules or aggregates of antibody molecules) revealed an apparent resolution of 42 nm.

Mechanism of Endocytosis - The co-distribution of Panx1 and proteins involved in clathrin or caveolin-mediated endocytosis in either 500 μM ATP or vehicle control treated N2a cells was evaluated using Pearson's correlation coefficient for Panx1—EGFP and antibodies for these proteins. Pearson's correlation coefficient is a pixel-by-pixel measure of the covariance in the intensities of two fluorophores. Pearson's values can range from 1 for linearly related distribution of two intensities to –1 for two intensities that have a perfectly inverse relationship, a value of 0 reflects an uncorrelated relationship [24]. Following an 8 h CHX treatment, cells were fixed at 30 min post-stimulus and co-distribution data were collected for each Panx1—EGFP-positive cell in a region of interest within 1 μm of any unopposed plasma membrane. The data for ≥ 50 cells was averaged for each biological replicate (N = 4). To assay for dynamin-dependent endocytosis, stable Panx1—EGFP N2a cells grown on PDL-coated coverslips were first incubated for 6 h in complete DMEM/F12 containing CHX. The cells were then rinsed and incubated in DMEM/F12 containing CHX supplemented with 2 mg/mL BSA for 1 h (all at 37 °C). Cells were then incubated for an additional hour in DMEM/F12/CHX/BSA supplemented with 80 μM Dynasore (Sigma-Aldrich) or DMSO control. Following this, cells were pre-incubated at 4 °C for 10 min, then in the same media supplemented 80 μM Dynasore or DMSO control and 25 μg/mL transferrin-Alexa Fluor 647 (Life Technologies) for an additional 45 min at 4 °C. Cells were then rinsed in ice-cold DMEM/F12/CHX/BSA supplemented with 80 μM Dynasore or DMSO control and fixed immediately or media was replaced with warm media containing 500 μM ATP or vehicle control. Following a 30 min incubation period at 37 °C (internalization period), cells were fixed, and intracellular Panx1—EGFP and transferrin were measured as described above.

Subcellular Distribution - The co-distribution of internalized Panx1—EGFP with antibody markers for specific subcellular compartments was determined by analysis of confocal micrographs with the Leica Application Suite software (version 3.1.3) Pearson's correlation tool. Following 8 h of CHX treatment, cells were fixed at 0.5, 1, and/or 2 h after 500 μM ATP stimulus. Vehicle-treated cells (2 h) served as control. Panx1—EGFP -expressing N2a cells were then immunostained with antibodies for subcellular compartment-specific markers. Images were

obtained at 4x optical zoom in 1024 x 1024 format with a pixel area of 71.02 nm^2 at room temperature using a 40x (1.3 NA) oil immersion objective as z-stacks and quantification was performed in the confocal plane displaying the largest central plane of the nucleus (Hoechst 33342) in the region of interest. For this analysis we re-named the intracellular analysis region as 'central' and we added a 1 μm thick region of analysis, termed 'peripheral', immediately outside the 'central' region (and bounded by the plasma membrane) because early endosomes are primarily located in the cell periphery (reviewed in [25]). The Pearson's correlation coefficient of Panx1—EGFP and antibodies for subcellular compartment-specific markers was determined per cell in each region of interest. The data for ≥ 50 cells were averaged for each biological replicate (N = 4).

Western blotting – N2a cells stably expressing Panx1—EGFP were treated with CHX, as described above in the live cell confocal experiments. Cells were either collected immediately (0 h) or stimulated with vehicle-control for 2 h or with ATP for 0.5, 1, or 2 h, and collected at the endpoint. Cells were homogenized in a Tris-based lysis buffer (150 mM NaCl, 1.0% IGEPAL CA-630, 0.5% sodium deoxycholate, 0.1% SDS, 50 mM Tris, pH 8.0), supplemented with protease inhibitor cocktail at 1 μL/10^6 cells (stock: 0.104 mM 4-(2-aminoethyl) benzenesulfoyl fluoride hydrochloride, 0.08 mM aprotinin, 4 mM bestatin hydrochloride, 1.4 mM n-(trans-epoxysuccinyl)-L-leucine 4-guanidinobutylamide, 2 mM leupeptin hemisulfate salt, 1.5 mM pepstatin A; Sigma-Aldrich), PMSF at 2 μL/10^6 cells, sodium orthovanadate at 2 μL/10^6 cells, and 1 mM EDTA and incubated on ice for 30 min. Homogenates were then passed through a 27-gauge needle three times and centrifuged at 17500 *g* for 15 min. Supernatant was collected as whole cell lysate. Samples were boiled (100 °C) for 20 min in SDS-PAGE loading dye under reducing conditions (DTT and β-mercaptoethanol). Western analysis was performed as previously described [2, 3, 26].

Reverse transcriptase-polymerase chain reaction (RT-PCR) **-** Total RNA was isolated and first-strand synthesis (Superscript II; according to the manufacturer's protocol; Life Technologies) was performed followed by PCR using cycling parameters of 94 °C for 5 min, 35 cycles of 94 °C for 30 sec, 55 °C for 30 sec, and 72 °C for 1 min, and a final step at 72 °C for 7 min for the following primers: 5′ -CTTGGCCTTCATTGCGGGTA-3′ , 5′ -GGAAGGCAAGACCATTAGGCA-3′ defining a 100-bp Cav-2 amplicon, accession number [GenBank: NM_016900] and 5′ -TGGTGCTGAGTATGTCGTGGAGT-3′ , 5′ -AGTCTTCTGAGTGGCAGTGATGG-3′ defining a 292 bp glyceraldehyde-3-phosphate dehydrogenase (GAPDH) amplicon, accession number [GenBank: NM_008084.2], while the cycling parameters of 94 °C for 5 min, 35 cycles of 94 °C for 30 sec, 53 °C for 30 sec, and 72 °C for 1 min, and a final step at 72 °C for 7 min were used for the primers 5'-CATGTCTGGGGGCAAATACG-3', 5'-GTCGTTGAGATGCTTGGGGT-3' defining a 184 bp Cav-1 amplicon, accession number [GenBank: NM_007616.4].

Statistical Analysis - Western blot densitometry was quantified using ImageJ 1.45 (http://rsbweb.nih.gov/ij/index.html). Significance was determined using unpaired Student's *t* tests. Results from live cell imaging experiments were analysed using a two-way ANOVA for time and treatment. Fixed cell confocal microscopy results were analysed using a one-way ANOVA or a Student's t test, where applicable. Data analysed using ANOVA were subsequently subjected to a Dunnett's post-hoc test, a multiple comparison procedure that compares all treatments to a single control. All data are presented as mean ± S.E.M.

RESULTS AND DISCUSSION

We tracked the movement of Panx1 in response to ATP in living N2a cells (Figure 1). These cells have a large cytoplasm to nucleus ratio, facilitating visualization of channel internalization. To create a relatively homogeneous, relatively low level of Panx1—EGFP, we established a Panx1—EGFP stable line that we pre-treated with the protein synthesis inhibitor CHX to eliminate a potential confounding fluorescence signal from *de novo* Panx1—EGFP in the secretory pathway (Figure 1A). We then used confocal microscopy to image Panx1—EGFP trafficking dynamics over a period of 25 min in the presence of ATP (0, 100, 200, 500 μM; Figure 1Bi). Supplementary Movie S1 clearly demonstrates the Panx1—EGFP signal overlapping with the red fluorescence signal of the labelled plasma membrane marker wheat-germ agglutinin (WGA), producing yellow vesicles internalizing from the plasma membrane in response to treatment with 500 μM ATP. To quantify intracellular Panx1, a trace was drawn 1 μm inside the WGA-defined plasma membrane to compute the average EGFP fluorescence intensity of the encapsulated area (Figure 1Bii). ATP triggered a significant time (≥15 min)- and dose (≥200 μM)-dependent increase in intracellular Panx1 after stimulation (Figure 1Biii). No significant increase in Panx1 internalization was detected with control treatment. A small, non-significant increase was observed with 100 μM ATP treatment. ATP treatment did not have an appreciable effect on cell size and shape or viability. To investigate if the effect was specific to the ATP stimulus directly, or could be attributed to a generalised increase in excitability triggered by the ATP stimulus, we compared 30 min ATP treatment with exposure to more generalised stimuli associated with increased excitability and/or excito-toxicity (Figure 1C). Following the treatment, the cells were fixed and intracellular Panx1 levels were measured by confocal microscopy. As expected from the live cell assay, treatment with 200 μM ATP elicited a significant increase in intracellular Panx1 (~180% of control), while K^+, OGD, and A23187 Ca^{2+} ionophore treatment did not significantly increase the intracellular population of Panx1. Although our earlier observations [27] suggested that these general stimuli can weakly influence Panx1 motility or surface expression they did not have a long lasting effect on the size of the internal pool of Panx1. These data are further supported by a biochemical cell surface luminometry assay in HEK293T cells [28] (Supplementary Figure 1). This assay requires a primary antibody to an extracellular epitope of the protein of interest. Abundance of the target protein is then measured by ECL with a standard plate reader. The signal from unpermeabilized cells (channels at the surface membrane) is normalized to the signal from permeabilized cells (channels on all cell membranes) to obtain a relative measure of channel cell surface expression amongst different treatments/experimental groups. We treated HEK293T cells overexpressing Panx1—EGFP with K^+ (10 mM), ATP (200 μM) or vehicle control. Cells were then processed for detection of surface and whole cell Panx1 using an antibody that recognizes an epitope in its second extracellular loop [21]. We found that ATP treatment (at a concentration associated with Panx1 channel inhibition [29, 30]) significantly decreased surface Panx1 compared to control, whereas elevated extracellular K^+ had no effect.

Next we sought to determine the nucleotide (nt) dependence of the effect, and relatedly, the possible involvement of purinergic receptors. Numerous studies have described functional and physical interactions of Panx1 with purinergic P2 receptors in various systems [31-36]. Screening the nt dependency of this effect can simultaneously provide insight into potential ionotropic (P2X) and metabotropic (P2Y) purinergic receptor involvement by capitalizing on the differential potency of different nt analogues. Following a 30-min incubation with the indicated nts (Figure 2), we fixed the cells and measured intracellular Panx1 levels using confocal

microscopy. In comparison with control treated cells, 500 μM ATP elicited a significant increase in intracellular Panx1 to ~280% of control (Figure 2A); whereas treatment with the slowly hydrolyzable ATP analogue, ATPγS (500 μM; P2X receptors) elicited a significant but smaller increase in intracellular Panx1 levels (~150% of control). The increase in intracellular Panx1 elicited by the slowly hydrolyzable ADP analogue, ADPβS (500 μM; P2Y receptors) was not significantly different from control-treated cells. In comparison with control, BzATP (P2X receptors) had a small but non-significant effect on Panx1 internalization (Figure 2B), while UTP (P2Y receptors) had no effect. These results suggest a lack of involvement of P2Y receptors: ADPβS and UTP, the two analogues that act on P2Y receptors [37-39], had no effect on Panx1 internalization. Further supporting a lack of P2Y involvement, the previously described mode of Panx1 activation via P2Y receptors involved a P2Y-mediated increase in intracellular Ca^{2+}, which can be mimicked by Ca^{2+} ionophore treatment. As demonstrated by the data presented in Figure 1, Ca^{2+} ionophore treatment had no effect on Panx1 internalization. The nt data were inconclusive with respect to P2X receptors. Because BzATP had a small albeit non-significant effect and since these cells express P2X4 and P2X7 receptors (with P2X7 being the primary functional isoform in these cells [40]), to rule out involvement of P2X receptors, we used the selective P2X7 blocker A438079 [41, 42]. Somewhat surprisingly, given the non-significant effect of BzATP, A438079 completely blocked Panx1 internalization. Despite the enigmatic nt dependence, this result implicates P2X7 receptors in ATP-stimulated Panx1 internalization.

Putative ATP-sensitive residues have also been identified within the Panx1 extracellular loops ([29, 30], reviewed in [43]). Qiu and Dahl [29, 30, 43] identified these in the course of investigating inhibition of Panx1 currents by ATP (≥200 μM) using *in vitro* expression systems. One of the residues at which ATP had a large effect was a tryptophan residue at amino acid 74 in the first extracellular loop of Panx1 [29]. To test the effect of this amino acid substitution on ATP-mediated Panx1 internalization, we generated the mutant EGFP-tagged construct, Panx1—W74—EGFP, and stably expressed it in N2a cells (Figure 3A). The ATP-insensitive Panx1 mutant (Panx1—W74—EGFP) exhibited robustly reduced ATP-mediated internalization (Figure 3B). In the Qiu and Dahl study first describing the ATP-sensitive residue W74A [29], the selective P2X7 blocker A438079 also inhibited Panx1 currents. Importantly, the expression systems used in studies of ATP inhibition of Panx1 currents [29, 30] endogenously express P2X receptors (*Xenopus* oocytes, HEK293T cells [44-46]). This suggests that the intrinsic ATP-sensitivity of Panx1 could involve interplay with P2X receptors. Note that there is no evidence, as of yet, that these are functionally expressed in *Xenopus* oocytes.

Next we sought to gain insight into the endocytosis mechanism (Figure 4). Endocytosis mechanisms are commonly classified into two major groups: clathrin-mediated endocytosis (CME), and clathrin-independent endocytosis (CIE); recently reviewed in [47]. Although CIE had historically been linked with a protein called caveolin, numerous caveolin-independent CIE mechanisms have now been described [47]. Because of its effects on membrane curvature and stability, cholesterol is known to play an important role in the majority of endocytic mechanisms [48]. To investigate the potential cholesterol dependence of ATP-stimulated Panx1 internalization, we first used Fil III, which binds to and aggregates cholesterol [49, 50]. In the presence of Fil III, ATP (500 μM) was not able to stimulate an increase in intracellular Panx1, whereas ATP had the expected effect in the presence of vehicle (an equal volume of DMSO; Figure 4A and 4B). To confirm the cholesterol dependence of internalization, we next employed the cholesterol-disrupting agent MβCD (Figure 4C), which acts by removing cholesterol from membranes [51]. MβCD also blocked Panx1 internalization, confirming the importance of

cholesterol. Therefore we next tested the effects of CLPZ (Figure 4D), a phenothiazine-derived antipsychotic drug (APD) and established CME inhibitor [52-54]. ATP-stimulated Panx1 internalization was preserved in the presence of CLPZ, suggesting that CME is not involved. To confirm these results we drew on previous work demonstrating that trans-membrane proteins employing caveolin-dependent CIE or CME mechanisms exhibit co-distribution with caveolin or clathrin [55] respectively. Consistent with previous reports [56, 57], we found that N2a cells express low levels of Cav-1, but we did not detect Cav-2 (Figure 4; Supplemental Figure S2). Note that the expression of a third caveolin, caveolin-3 is muscle-specific [58]. We found that Panx1 did not strongly co-distribute with either Cav-1 or clathrin heavy chain. We quantitatively examined co-distribution of Panx1 with Cav-1 (Figure 4E) and clathrin heavy chain (Figure 4F) following ATP stimulus. To confirm our data suggesting the mechanism of Panx1 internalization is independent of both CME and caveolin-dependent CIE pathways, we capitalized on the fact that CME and caveolin-dependent CIE converge mechanistically at the dynamin-dependent scission step. We therefore used the pharmacological inhibitor of dynamin I, dynamin II and mitochondrial dynamin, Dynasore [59, 60]. We observed similar significant ATP-induced increases in intracellular Panx1 in the presence of Dynasore or vehicle control (Figure 5C). Together these data suggest that ATP-stimulated Panx1 internalization is dependent on cholesterol, but is probably independent of dynamin, pointing to a non-caveolin CIE mechanism. The study of non-caveolin CIE pathways involving ion channels and receptors is complex and rapidly evolving [47]. Given that Panx1 was recently identified as a ubiquitinated protein [61], which is a key CIE mechanism [62], the putative role of ubiquitination (and associated protein machinery) in ATP-dependent Panx1 internalization will be the focus of future study. Consistent with our results, an earlier report [63] demonstrated that basal (un-stimulated) Panx1 internalization did not occur by CME or caveolin-dependent CIE. However, in contrast with our findings on stimulated internalization, basal internalization was unaffected by the cholesterol disruptor MβCD. It is reasonable to speculate that Panx1 could be internalized through different pathways depending on the context (basal compared with stimulated) as has been observed with other proteins [47].

Since internalized surface proteins are often targeted for degradation, we examined whole-cell Panx1—EGFP (in the presence of CHX) in ATP treated (0.5, 1 and 2 h after treatment) and control vehicle treated cells (0 and 2 h after treatment). Figure 6(A) demonstrates that overall Panx1 levels (normalized to β-actin levels) were unchanged throughout the analysis period in both control and ATP-treated cells suggesting that internalized Panx1 is not targeted for degradation over this 2 h period. We next sought to determine Panx1's intracellular destination over time (0.5, 1 and 2 h) after 500 μM ATP stimulation by measuring Pearson's correlation coefficient for Panx1 and the markers outlined in Figure 6(B). Upon internalization from the plasma membrane, transmembrane proteins first encounter the early endosome (EEA1). From there they can follow the degradation pathway, through the late endosome (Rab7 [64]) and endolysosome (M6PR [65, 66]) to end up in the lysosome (Lamp1 [67]) or they can be diverted from the early endosome to recycling endosomes (Rab14 [68, 69], Rab11, Rab4 [70]) with potential to return to the plasma membrane. Transmembrane proteins also shuttle to and from the *trans*-Golgi network (giantin [71]). Supplementary Figure S3 demonstrates that, in N2a cells, these markers can be spatially distinguished from one another using confocal microscopy. As expected, EEA1 and giantin demonstrated limited co-distribution (Pearson's: 0.029±0.003). EEA1 and Lamp1 shared minor co-distribution (Pearson's: 0.16±0.01). Although these are at opposite ends of the degradation pathway, one would expect a degree of overlap reflecting the

constant membrane trafficking between the various endosomal compartments and the lysosome during endosomal maturation [25]. As anticipated given their shared localization within recycling endosomes, Rab4 and Rab14 had a much higher degree of co-distribution (0.53±0.03).

Reflecting the peripheral to central distribution of endosomes with progression through the degradation pathway (reviewed in [25]), we defined an additional 1 μm thick region of analysis, 'peripheral', immediately outside the intracellular region (defined in Figure 1) that we newly defined here as 'central'. We anticipated that 0.5 h after ATP treatment we would expect to see increased Panx1 at the most immature early endosomes, and that we could potentially miss this observation if we did not add this peripheral region of analysis where the most immature early endosomes are most likely to be found. Given the limits of resolution of light microscopy, we would expect this 'peripheral' region to include populations of Panx1 (1) at the plasma membrane, (2) immediately beneath the plasma membrane and (3) in peripherally-located early endosomes. As expected, 0.5 h following ATP treatment peripheral Panx1/EEA1 co-distribution was significantly increased (~150%) in comparison with control treated cells (Figure 6C). Moreover, higher resolution STED microscopy confirmed the localization of Panx1 to EEA1-positive early endosomes (Figure 5Ciii). At the same time point, there was a significant decrease (by ~50%) in central Panx1/Rab7 and Panx1/Lamp1 co-distribution (Supplementary Figure S4), suggesting the sub-population of Panx1 in the degradation pathway is decreasing in response to increased extracellular ATP. At 1 h after ATP treatment, central Panx1/Rab14 co-distribution significantly increased (~220%) relative to control and remained high (~240%) at 2 h (Figure 5D). The localization of Panx1 at Rab14-positive recycling endosomes was confirmed with STED microscopy (Figure 6Diii). Additional recycling endosome markers Rab11 and Rab4 exhibited a similar result as Rab14, albeit non-significant for Rab4 (Supplementary Figure S4). This sub-population of Panx1 in the recycling endosome could either be en-route to return to the plasma membrane or could be recruited to the recycling endosome to play a yet-to-be-determined functional role therein.

Our analysis also revealed that under control conditions intracellular Panx1, when present, co-distributed most strongly with markers for the early endosome, late endosome, endolysosome and the lysosome (Supplementary Figure S4). These results suggest a sub-population of intracellular Panx1 is expressed in endosomes under control conditions and primarily localizes to the degradation pathway. Here, Panx1 could either play a functional role, as suggested by a recent study demonstrating the Panx1 blocker probenecid blocks lysosome function [72] or simply be constitutively targeted for degradation. We did not see a reduction in Panx1 over the 2 h observation period in this study; however, previous work indicated that disruption of the lysosome led to accumulation of Panx1 [63] (albeit in a different cell line). A longer analysis period in future studies will help to resolve this potential discrepancy. Note that Panx1 exhibited limited expression in the Golgi under control conditions, thus the physiological relevance of the significant relative decrease in co-distribution with giantin at 0.5 h with ATP treatment is uncertain (Supplementary Figure S4). Together these results suggest that ATP stimulus increases the trafficking of a subpopulation of Panx1 to recycling endosomes.

Our results, in the present study, identify a novel localization of intracellular Panx1 within endosomal systems and raise important considerations with regards to Panx1 surface stability in diverse physiological and pathophysiological scenarios in which ATP can be rapidly elevated in the extracellular space. In the presence of elevated extracellular ATP, intracellular Panx1 is increased and the co-distribution of Panx1 with markers for recycling endosomes is increased. ATP is episodically released from developing neurons in the ventricular zone of the

lateral ventricles, acting as an important autocrine and paracrine regulator of their proliferation, differentiation and migration through activation of various purinergic receptors that are developmentally regulated [18, 19]. Furthermore, ATP is co-released with other neurotransmitters as an important modulator of synaptic plasticity and is also released from immune cells and dead and dying cells; recently reviewed in [73]. Locally surrounding the ATP release sites (from vesicle/granule release or ATP-permeable channels), ATP levels would be predicted to be very high, analogous to Ca^{2+} micro and nano domains surrounding Ca^{2+}-permeable channels [74, 75]. Intracellular ATP concentrations range from 3 to 5 mM, and secretory vesicles can contain ATP on the order of 100 mM (reviewed in [76] and see also [77]). Consequently, taking into account extracellular nucleotidase activity, ATP levels would be comparable to those tested in this study (if not higher) in the microdomain surrounding vesicular release sites or ATP channels. It is reasonable to propose that in the context of Panx1 as an ATP-release channel, ATP-mediated internalization of Panx1 could represent an important homeostatic means of regulating ATP release within a range of extracellular concentrations.

A putative functional role of Panx1 in the degradation and recycling endosome systems remains to be determined. A recent report demonstrated neuroprotection in the context of stroke was contingent on double knockout of both Panx1 and Panx2, suggesting functional overlap [78, 79]. This suggests there could be a crosstalk between Panx1 and resident Panx2 [15, 26, 80, 81] in endolysosomal membranes. Interestingly, Boassa et al. [80], observed no co-distribution between Panx1 and Panx2 (in MDCK, HeLa, and HEK293T cells), but did observe co-distribution between Panx2 and Rab4. Our data suggest that in N2a cells, Panx1 and Panx2 could co-distribute in Rab4-positive endosomes and potentially other endosomal compartments that were not explored in that study. Whether Panx1 and Panx2 physically or functionally co-operate in one or both of the endosomal systems remains to be determined.

Overall this study enhances our understanding of the localization of Panx1 within cells and the factors that contribute to the regulation of Panx1 channel trafficking. These novel findings have significant implications for scenarios in which extracellular ATP levels are dynamic. Based on our pharmacological data with the selective P2X7 receptor blocker A438079, our data suggest that P2X7 receptors could be involved in ATP-stimulated Panx1 internalization, possibly in combination with putative ATP-sensitive residues in the Panx1 sequence. This suggests that a similar internalization phenomenon could be expected in cells expressing both Panx1 and P2X7 receptors, as was the case with our N2a cell and HEK293T cell assays. The important next steps will be to understand the precise contribution and mechanisms of P2X7 receptor involvement as well as their interplay with ATP-sensitive residues in Panx1, and to extend these results into *in vivo* systems.

REFERENCES

1 Penuela, S., Gehi, R. and Laird, D. W. (2013) The biochemistry and function of pannexin channels. Biochim Biophys Acta. **1828**, 15-22

2 Wicki-Stordeur, L. E., Dzugalo, A. D., Swansburg, R. M., Suits, J. M. and Swayne, L. A. (2012) Pannexin 1 regulates postnatal neural stem and progenitor cell proliferation. Neural Dev. **7**, 11

3 Wicki-Stordeur, L. E. and Swayne, L. A. (2013) Panx1 regulates neural stem and progenitor cell behaviours associated with cytoskeletal dynamics and interacts with multiple cytoskeletal elements. Cell Commun Signal. **11**, 62

4 Ray, A., Zoidl, G., Weickert, S., Wahle, P. and Dermietzel, R. (2005) Site-specific and developmental expression of pannexin1 in the mouse nervous system. Eur J Neurosci. **21**, 3277-3290
5 Vogt, A., Hormuzdi, S. G. and Monyer, H. (2005) Pannexin1 and Pannexin2 expression in the developing and mature rat brain. Brain Res Mol Brain Res. **141**, 113-120
6 Iglesias, R., Dahl, G., Qiu, F., Spray, D. C. and Scemes, E. (2009) Pannexin 1: the molecular substrate of astrocyte "hemichannels". J Neurosci. **29**, 7092-7097
7 Suadicani, S. O., Iglesias, R., Wang, J., Dahl, G., Spray, D. C. and Scemes, E. (2012) ATP signaling is deficient in cultured Pannexin1-null mouse astrocytes. Glia. **60**, 1106-1116
8 Prochnow, N., Abdulazim, A., Kurtenbach, S., Wildforster, V., Dvoriantchikova, G., Hanske, J., Petrasch-Parwez, E., Shestopalov, V. I., Dermietzel, R., Manahan-Vaughan, D. and Zoidl, G. (2012) Pannexin1 stabilizes synaptic plasticity and is needed for learning. PLoS One. **7**, e51767
9 Ardiles, A. O., Flores-Munoz, C., Toro-Ayala, G., Cardenas, A. M., Palacios, A. G., Munoz, P., Fuenzalida, M., Saez, J. C. and Martinez, A. D. (2014) Pannexin 1 regulates bidirectional hippocampal synaptic plasticity in adult mice. Front Cell Neurosci. **8**, 326
10 Thompson, R. J., Zhou, N. and MacVicar, B. A. (2006) Ischemia Opens Neuronal Gap Junction Hemichannels. Science. **312**, 924-927
11 Weilinger, N. L., Tang, P. L. and Thompson, R. J. (2012) Anoxia-induced NMDA receptor activation opens pannexin channels via Src family kinases. J Neurosci. **32**, 12579-12588
12 Cheung, G., Chever, O. and Rouach, N. (2014) Connexons and pannexons: newcomers in neurophysiology. Front Cell Neurosci. **8**, 348
13 Thompson, R. J. (2014) Pannexin channels and ischaemia. J Physiol. **[Epub ahead of print]**
14 Penuela, S., Celetti, S. J., Bhalla, R., Shao, Q. and Laird, D. W. (2008) Diverse subcellular distribution profiles of pannexin 1 and pannexin 3. Cell Commun Adhes. **15**, 133-142
15 Cone, A. C., Ambrosi, C., Scemes, E., Martone, M. E. and Sosinsky, G. E. (2013) A comparative antibody analysis of pannexin1 expression in four rat brain regions reveals varying subcellular localizations. Frontiers in pharmacology. **4**, 6
16 Lai, C. P., Bechberger, J. F., Thompson, R. J., MacVicar, B. A., Bruzzone, R. and Naus, C. C. (2007) Tumor-suppressive effects of pannexin 1 in C6 glioma cells. Cancer Res. **67**, 1545-1554
17 Vanden Abeele, F., Bidaux, G., Gordienko, D., Beck, B., Panchin, Y. V., Baranova, A. V., Ivanov, D. V., Skryma, R. and Prevarskaya, N. (2006) Functional implications of calcium permeability of the channel formed by pannexin 1. J Cell Biol. **174**, 535-546
18 Lin, J. H., Takano, T., Arcuino, G., Wang, X., Hu, F., Darzynkiewicz, Z., Nunes, M., Goldman, S. A. and Nedergaard, M. (2007) Purinergic signaling regulates neural progenitor cell expansion and neurogenesis. Dev Biol. **302**, 356-366
19 Mishra, S. K., Braun, N., Shukla, V., Fullgrabe, M., Schomerus, C., Korf, H. W., Gachet, C., Ikehara, Y., Sevigny, J., Robson, S. C. and Zimmermann, H. (2006) Extracellular nucleotide signaling in adult neural stem cells: synergism with growth factor-mediated cellular proliferation. Development. **133**, 675-684
20 Penuela, S., Bhalla, R., Gong, X.-Q., Cowan, K. N., Celetti, S. J., Cowan, B. J., Bai, D., Shao, Q. and Laird, D. W. (2007) Pannexin 1 and pannexin 3 are glycoproteins that exhibit many distinct characteristics from the connexin family of gap junction proteins. J Cell Sci. **120**, 3772-3783

21 Penuela, S., Bhalla, R., Nag, K. and Laird, D. W. (2009) Glycosylation regulates pannexin intermixing and cellular localization. Mol Biol Cell. **20**, 4313-4323
22 Klar, T. A., Jakobs, S., Dyba, M., Egner, A. and Hell, S. W. (2000) Fluorescence microscopy with diffraction resolution barrier broken by stimulated emission. Proc Natl Acad Sci U S A. **97**, 8206-8210
23 Schoonderwoert, V. T., Dijkstra, R., Luckinavicius, G., Kobler, O. and Van der Voort, H. (2013) Huygens STED Deconvolution Increases Signal-to-Noise and Image Resolution towards 22 nm. Microscopy Today. **21**, 38-44
24 Dunn, K. W., Kamocka, M. M. and McDonald, J. H. (2011) A practical guide to evaluating colocalization in biological microscopy. Am J Physiol Cell Physiol. **300**, C723-742
25 Huotari, J. and Helenius, A. (2011) Endosome maturation. EMBO J. **30**, 3481-3500
26 Swayne, L. A., Sorbara, C. D. and Bennett, S. A. (2010) Pannexin 2 is expressed by postnatal hippocampal neural progenitors and modulates neuronal commitment. J Biol Chem. **285**, 24977-24986
27 Boyce, A. K., Prager, R. T., Wicki-Stordeur, L. E. and Swayne, L. A. (2013) Pore positioning: Current concepts in Pannexin channel trafficking. Channels (Austin). **8**
28 Dubel, S. J., Altier, C., Chaumont, S., Lory, P., Bourinet, E. and Nargeot, J. (2004) Plasma Membrane Expression of T-type Calcium Channel {alpha}1 Subunits Is Modulated by High Voltage-activated Auxiliary Subunits. Journal of Biological Chemistry. **279**, 29263-29269
29 Qiu, F., Wang, J. and Dahl, G. (2012) Alanine substitution scanning of pannexin1 reveals amino acid residues mediating ATP sensitivity. Purinergic Signal. **8**, 81-90
30 Qiu, F. and Dahl, G. (2009) A permeant regulating its permeation pore: inhibition of pannexin 1 channels by ATP. Am J Physiol Cell Physiol. **296**, C250-255
31 Iglesias, R., Locovei, S., Roque, A., Alberto, A. P., Dahl, G., Spray, D. C. and Scemes, E. (2008) P2X7 receptor-Pannexin1 complex: pharmacology and signaling. Am J Physiol Cell Physiol. **295**, C752-760
32 Pelegrin, P. and Surprenant, A. (2006) Pannexin-1 mediates large pore formation and interleukin-1beta release by the ATP-gated P2X7 receptor. EMBO J. **25**, 5071-5082
33 Locovei, S., Scemes, E., Qiu, F., Spray, D. C. and Dahl, G. (2007) Pannexin1 is part of the pore forming unit of the P2X(7) receptor death complex. FEBS Lett. **581**, 483-488
34 Maslieieva, V. and Thompson, R. J. (2014) A critical role for pannexin-1 in activation of innate immune cells of the choroid plexus. Channels (Austin). **8**, 131-141
35 Shoji, K. F., Saez, P. J., Harcha, P., Aguila, H. L. and Saez, J. C. (2014) Pannexin1 channels act downstream of P2X receptors in ATP-induced murine T-cell death. Channels (Austin). **8**
36 Kanjanamekanant, K., Luckprom, P. and Pavasant, P. (2014) P2X7 receptor-Pannexin1 interaction mediates stress-induced interleukin-1 beta expression in human periodontal ligament cells. Journal of periodontal research. **49**, 595-602
37 von Kugelgen, I. (2006) Pharmacological profiles of cloned mammalian P2Y-receptor subtypes. Pharmacol Ther. **110**, 415-432
38 Jacobson, K. A., Balasubramanian, R., Deflorian, F. and Gao, Z. G. (2012) G protein-coupled adenosine (P1) and P2Y receptors: ligand design and receptor interactions. Purinergic Signal. **8**, 419-436
39 Weisman, G. A., Woods, L. T., Erb, L. and Seye, C. I. (2012) P2Y receptors in the mammalian nervous system: pharmacology, ligands and therapeutic potential. CNS Neurol Disord Drug Targets. **11**, 722-738

40 Gomez-Villafuertes, R., del Puerto, A., Diaz-Hernandez, M., Bustillo, D., Diaz-Hernandez, J. I., Huerta, P. G., Artalejo, A. R., Garrido, J. J. and Miras-Portugal, M. T. (2009) Ca2+/calmodulin-dependent kinase II signalling cascade mediates P2X7 receptor-dependent inhibition of neuritogenesis in neuroblastoma cells. FEBS J. **276**, 5307-5325
41 McGaraughty, S., Chu, K. L., Namovic, M. T., Donnelly-Roberts, D. L., Harris, R. R., Zhang, X. F., Shieh, C. C., Wismer, C. T., Zhu, C. Z., Gauvin, D. M., Fabiyi, A. C., Honore, P., Gregg, R. J., Kort, M. E., Nelson, D. W., Carroll, W. A., Marsh, K., Faltynek, C. R. and Jarvis, M. F. (2007) P2X7-related modulation of pathological nociception in rats. Neuroscience. **146**, 1817-1828
42 Nelson, D. W., Gregg, R. J., Kort, M. E., Perez-Medrano, A., Voight, E. A., Wang, Y., Grayson, G., Namovic, M. T., Donnelly-Roberts, D. L., Niforatos, W., Honore, P., Jarvis, M. F., Faltynek, C. R. and Carroll, W. A. (2006) Structure-activity relationship studies on a series of novel, substituted 1-benzyl-5-phenyltetrazole P2X7 antagonists. J Med Chem. **49**, 3659-3666
43 Dubyak, G. R. (2009) Both sides now: multiple interactions of ATP with pannexin-1 hemichannels. Focus on "A permeant regulating its permeation pore: inhibition of pannexin 1 channels by ATP". Am J Physiol Cell Physiol. **296**, C235-241
44 Juranka, P. F., Haghighi, A. P., Gaertner, T., Cooper, E. and Morris, C. E. (2001) Molecular cloning and functional expression of Xenopus laevis oocyte ATP-activated P2X4 channels. Biochim Biophys Acta. **1512**, 111-124
45 Worthington, R. A., Dutton, J. L., Poronnik, P., Bennett, M. R. and Barden, J. A. (1999) Localisation of P2X receptors in human salivary gland epithelial cells and human embryonic kidney cells by sodium dodecyl sulfate-polyacrylamide gel electrophoresis/Western blotting and immunofluorescence. Electrophoresis. **20**, 2065-2070
46 Ma, W., Hui, H., Pelegrin, P. and Surprenant, A. (2009) Pharmacological characterization of pannexin-1 currents expressed in mammalian cells. J Pharmacol Exp Ther. **328**, 409-418
47 Maldonado-Baez, L., Williamson, C. and Donaldson, J. G. (2013) Clathrin-independent endocytosis: a cargo-centric view. Exp Cell Res. **319**, 2759-2769
48 Rodal, S. K., Skretting, G., Garred, O., Vilhardt, F., van Deurs, B. and Sandvig, K. (1999) Extraction of cholesterol with methyl-beta-cyclodextrin perturbs formation of clathrin-coated endocytic vesicles. Mol Biol Cell. **10**, 961-974
49 Rothberg, K. G., Ying, Y. S., Kamen, B. A. and Anderson, R. G. (1990) Cholesterol controls the clustering of the glycophospholipid-anchored membrane receptor for 5-methyltetrahydrofolate. J Cell Biol. **111**, 2931-2938
50 Rothberg, K. G., Heuser, J. E., Donzell, W. C., Ying, Y. S., Glenney, J. R. and Anderson, R. G. (1992) Caveolin, a protein component of caveolae membrane coats. Cell. **68**, 673-682
51 Klein, U., Gimpl, G. and Fahrenholz, F. (1995) Alteration of the myometrial plasma membrane cholesterol content with beta-cyclodextrin modulates the binding affinity of the oxytocin receptor. Biochemistry. **34**, 13784-13793
52 Sofer, A. and Futerman, A. H. (1995) Cationic amphiphilic drugs inhibit the internalization of cholera toxin to the Golgi apparatus and the subsequent elevation of cyclic AMP. J Biol Chem. **270**, 12117-12122
53 Vendeville, A., Rayne, F., Bonhoure, A., Bettache, N., Montcourrier, P. and Beaumelle, B. (2004) HIV-1 Tat enters T cells using coated pits before translocating from acidified endosomes and eliciting biological responses. Mol Biol Cell. **15**, 2347-2360

54 Okamoto, Y., Ninomiya, H., Miwa, S. and Masaki, T. (2000) Cholesterol oxidation switches the internalization pathway of endothelin receptor type A from caveolae to clathrin-coated pits in Chinese hamster ovary cells. J Biol Chem. **275**, 6439-6446
55 Rappoport, J. Z. and Simon, S. M. (2009) Endocytic trafficking of activated EGFR is AP-2 dependent and occurs through preformed clathrin spots. J Cell Sci. **122**, 1301-1305
56 Kang, Y. S., Zhao, X., Lovaas, J., Eisenberg, E. and Greene, L. E. (2009) Clathrin-independent internalization of normal cellular prion protein in neuroblastoma cells is associated with the Arf6 pathway. J Cell Sci. **122**, 4062-4069
57 Madeira, A., Yang, J., Zhang, X., Vikeved, E., Nilsson, A., Andren, P. E. and Svenningsson, P. (2011) Caveolin-1 interacts with alpha-synuclein and mediates toxic actions of cellular alpha-synuclein overexpression. Neurochem Int. **59**, 280-289
58 Williams, T. M. and Lisanti, M. P. (2004) The Caveolin genes: from cell biology to medicine. Ann Med. **36**, 584-595
59 Macia, E., Ehrlich, M., Massol, R., Boucrot, E., Brunner, C. and Kirchhausen, T. (2006) Dynasore, a cell-permeable inhibitor of dynamin. Dev Cell. **10**, 839-850
60 Kirchhausen, T., Macia, E. and Pelish, H. E. (2008) Use of dynasore, the small molecule inhibitor of dynamin, in the regulation of endocytosis. Methods Enzymol. **438**, 77-93
61 Kim, W., Bennett, E. J., Huttlin, E. L., Guo, A., Li, J., Possemato, A., Sowa, M. E., Rad, R., Rush, J., Comb, M. J., Harper, J. W. and Gygi, S. P. (2011) Systematic and quantitative assessment of the ubiquitin-modified proteome. Molecular cell. **44**, 325-340
62 Acconcia, F., Sigismund, S. and Polo, S. (2009) Ubiquitin in trafficking: the network at work. Exp Cell Res. **315**, 1610-1618
63 Gehi, R., Shao, Q. and Laird, D. W. (2011) Pathways regulating the trafficking and turnover of pannexin1 protein and the role of the C-terminal domain. The Journal of biological chemistry. **286**, 27639-27653
64 Vitelli, R., Santillo, M., Lattero, D., Chiariello, M., Bifulco, M., Bruni, C. B. and Bucci, C. (1997) Role of the small GTPase Rab7 in the late endocytic pathway. J Biol Chem. **272**, 4391-4397
65 Ghosh, P., Dahms, N. M. and Kornfeld, S. (2003) Mannose 6-phosphate receptors: new twists in the tale. Nature reviews. Molecular cell biology. **4**, 202-212
66 Brown, W. J., Goodhouse, J. and Farquhar, M. G. (1986) Mannose-6-phosphate receptors for lysosomal enzymes cycle between the Golgi complex and endosomes. J Cell Biol. **103**, 1235-1247
67 Eskelinen, E. L. (2006) Roles of LAMP-1 and LAMP-2 in lysosome biogenesis and autophagy. Mol Aspects Med. **27**, 495-502
68 Linford, A., Yoshimura, S., Nunes Bastos, R., Langemeyer, L., Gerondopoulos, A., Rigden, D. J. and Barr, F. A. (2012) Rab14 and its exchange factor FAM116 link endocytic recycling and adherens junction stability in migrating cells. Dev Cell. **22**, 952-966
69 Prekeris, R. (2012) The art of "cut and run": the role of Rab14 GTPase in regulating N-cadherin shedding and cell motility. Dev Cell. **22**, 909-910
70 Sonnichsen, B., De Renzis, S., Nielsen, E., Rietdorf, J. and Zerial, M. (2000) Distinct membrane domains on endosomes in the recycling pathway visualized by multicolor imaging of Rab4, Rab5, and Rab11. J Cell Biol. **149**, 901-914
71 Linstedt, A. D. and Hauri, H. P. (1993) Giantin, a novel conserved Golgi membrane protein containing a cytoplasmic domain of at least 350 kDa. Mol Biol Cell. **4**, 679-693

72 Wei, R., Wang, J., Xu, Y., Yin, B., He, F., Du, Y., Peng, G. and Luo, B. (2015) Probenecid protects against cerebral ischemia/reperfusion injury by inhibiting lysosomal and inflammatory damage in rats. Neuroscience. **301**, 168-177
73 Burnstock, G., Krugel, U., Abbracchio, M. P. and Illes, P. (2011) Purinergic signalling: from normal behaviour to pathological brain function. Progress in neurobiology. **95**, 229-274
74 Tadross, M. R., Tsien, R. W. and Yue, D. T. (2013) Ca2+ channel nanodomains boost local Ca2+ amplitude. Proc Natl Acad Sci U S A. **110**, 15794-15799
75 Neher, E. and Almers, W. (1986) Fast calcium transients in rat peritoneal mast cells are not sufficient to trigger exocytosis. EMBO J. **5**, 51-53
76 Dubyak, G. R. and el-Moatassim, C. (1993) Signal transduction via P2-purinergic receptors for extracellular ATP and other nucleotides. Am J Physiol. **265**, C577-606
77 Sawada, K., Echigo, N., Juge, N., Miyaji, T., Otsuka, M., Omote, H., Yamamoto, A. and Moriyama, Y. (2008) Identification of a vesicular nucleotide transporter. Proc Natl Acad Sci U S A. **105**, 5683-5686
78 Bargiotas, P., Krenz, A., Hormuzdi, S. G., Ridder, D. A., Herb, A., Barakat, W., Penuela, S., von Engelhardt, J., Monyer, H. and Schwaninger, M. (2011) Pannexins in ischemia-induced neurodegeneration. Proc Natl Acad Sci U S A. **108**, 20772-20777
79 Bargiotas, P., Krenz, A., Monyer, H. and Schwaninger, M. (2012) Functional outcome of pannexin-deficient mice after cerebral ischemia. Channels (Austin). **6**, 453-456
80 Boassa, D., Nguyen, P., Hu, J., Ellisman, M. H. and Sosinsky, G. E. (2014) Pannexin2 oligomers localize in the membranes of endosomal vesicles in mammalian cells while Pannexin1 channels traffic to the plasma membrane. Front Cell Neurosci. **8**, 468
81 Wicki-Stordeur, L. E., Boyce, A. K. and Swayne, L. A. (2013) Analysis of a pannexin 2-pannexin 1 chimeric protein supports divergent roles for pannexin C-termini in cellular localization. Cell communication & adhesion. **20**, 73-79

Abbreviations: ADPβS, adenosine-5'-(β-thio)-diphosphate; ATPγS, adenosine-5'-(γ-thio)-triphosphate; BzATP, 2'(3')-O-(4-benzoylbenzoyl) adenosine 5'-triphosphate; Cav-1/2; caveolin-1/2; CHX, cycloheximide; CIE, clathrin-independent endocytosis; CLPZ, chlorpromazine; CME, clathrin-mediated endocytosis; DMEM, Dulbecco's Modified Eagle's medium; EEA1, early endosomal antigen 1; EL2, extracellular loop 2; Fil III, filipin III; HEK293T, human embryonic kidney 293T; HRP, horseradish peroxidase; Lamp1, lysosomal-associated membrane protein 1; M6PR, mannose 6-phosphate receptor; MβCD, methyl-β-cyclodextrin; NA, numerical aperture; N2a, Neuro2a; OGD, oxygen glucose deprivation; P2X, ionotropic purinergic receptor; P2Y, metabotropic purinergic receptor; Panx1, pannexin 1; PDL, poly-D-lysine; Rab, Ras related protein Rab; STED, stimulated emission depletion; WGA, wheat germ agglutinin.

ACKNOWLEDGEMENTS
We thank Dr Silvia Penuela and Dr Dale Laird (Western University) for the Panx1—EGFP plasmid and the Panx1—EL2 antibody. We thank Reg Sidhu (Leica Microsystems) for providing access to the Leica TCS SP8 STED system.

FUNDING
This work was supported by operating grant support to L.A.S. from the Natural Sciences and Engineering Research Council (NSERC) [grant number 402270- 2011], and infrastructure

support from the Canadian Foundation for Innovation (CFI) [grant number 29462], and the BC Knowledge Development Fund (BCKDF) [grant number 804754]. L.A.S. was also supported by a salary grant from the Michael Smith Foundation for Health Research (MSFHR) [grant number 5900]. Student scholarships were awarded to A.K.J.B. from NSERC [grant number PGSD 459931-2014] and from the University of Victoria (President's Research Scholarship), to M.S.K. from NSERC (USRA**),** and to L.E.W.S. from NSERC (grant number Vanier Canada Graduate Scholarship CGV-NSERC- 00184).

AUTHOR CONTRIBUTIONS

Leigh Anne Swayne directed the study, wrote and revised the manuscript, helped to prepare the figures and performed the cell surface luminometry experiments. Andrew Boyce performed the majority of the experiments, prepared the figures and contributed to the writing and revision of the manuscript. Michelle Kim created the W74A mutant Panx1—EGFP construct. Leigh Wicki-Stordeur assisted with cell surface luminometry and cell culture.

FIGURE LEGENDS

Figure 1. Elevated extracellular ATP stimulates internalization of Panx1. (**A**) N2a cells stably expressing Panx1—EGFP were treated for 8 h with CHX (20 μg/mL) to observe the mature population of Panx1 and then stimulated with the indicated concentrations of ATP. (**B**) Representative confocal micrographs from the 0- and 25-min time points (**i**) and depiction of the region of analysis from the insets (**ii**, digital zoom). Intracellular Panx1 fluorescence intensity expressed as a percentage of time zero at each 5-min interval (**iii**). $N = 6$, two-way ANOVA [time: $F(4, 20) = 26.7$; treatment: $F(3, 20) = 8.35$; interaction: $F(12, 20) = 9.16$] with Dunnett's *post-hoc*. Scale bars = 10 μm. (**C**) Effects of 200 μM ATP, 30 mM K^+, 10 μM Ca^{2+} ionophore A23187 and chemical OGD (100 μM potassium cyanide and 1 μg/mL oligomycin) relative to vehicle control on intracellular Panx1 at 30 min post-stimulus. $N = 4$; one-way ANOVA with Dunnett's *post-hoc* test. *P <0.05, **P <0.01, ***P <0.001, ****P <0.0001.

Figure 2. Panx1 is selectively internalized by ATP and its slowly-hydrolyzable analogue ATPγS and is abrogated by the selective P2X7 inhibitor A438079. (**A**) Confocal micrographs of N2a cells stably expressing Panx1—EGFP 30 min following stimulation with vehicle control or ATP, ATPγS, or ADPβS (each 500 μM; **i**). Intracellular Panx1 was quantified relative to vehicle control (**ii**). $N = 4$, one-way ANOVA with Dunnett's *post-hoc* test. (**B**) Confocal micrographs of N2a cells stably expressing Panx1—EGFP 30 min following stimulation with vehicle control, 500 μM ATP, 100 μM BzATP or 500 μM UTP (**i**). Intracellular Panx1 was quantified in cells that had been stimulated with 100 or 500 μM ATP, 100 or 500 μM BzATP, or 500 μM UTP relative to vehicle control (**ii**). $N = 4$, one-way ANOVA with Dunnett's *post-hoc* test. (**C**) Confocal micrographs of N2a cells stably expressing Panx1—EGFP that were pre-treated for 1 h prior to 500 μM ATP or control treatment with 100 μM A438079 and fixed at 30 min post-stimulus (**i**). Intracellular Panx1 was quantified relative to vehicle control (**ii**). $N = 4$, one-way ANOVA with Dunnett's *post-hoc* test. ***P <0.001, ****P <0.0001. Hoechst (blue) was used as a nuclear counterstain.

Figure 3. ATP-dependent Panx1 internalization is impaired in Panx1—W74A-expressing cells. (**A**) The extent of intracellular Panx1 is demonstrated in confocal micrographs (**i**) of N2a cells stably expressing Panx1—EGFP (top panels) or mutant Panx1—W74A—EGFP (bottom panels) stimulated with vehicle control (left panels) or 500 μM ATP (right panels) for 30 min, quantified relative to control in (**ii**). $N = 4$, one-way ANOVA with Dunnett's *post-hoc* test. Scale bars = 10 μm. ****$P < 0.0001$. Hoechst (blue) was used as a nuclear counterstain.

Figure 4. Panx1 internalization is cholesterol-dependent and relies on clathrin and caveolin-independent endocytosis mechanisms. Intracellular Panx1 relative to control conditions in N2a cells stably expressing Panx1—EGFP incubated in vehicle control (**A**; DMSO), Fil III (**B**; 1 μg/mL), MβCD (**C**; 10 mM); or CLPZ (**D**; 10 μg/mL) for 1 h prior to treatment for 30 min with 500 μM ATP or vehicle control. Representative confocal images demonstrate distribution of Panx1—EGFP (green) in ATP and control-treated cells in the presence of each inhibitor or vehicle control. $N = 4$, Student's *t* test. Scale bars = 10 μm. (**E**) Confocal micrographs (**i**) of control (top panels) or ATP-treated (bottom panels) N2a cells stably expressing Panx1—EGFP immunostained for Cav-1 (red). Panx1—EGFP—Cav-1 co-distribution in control and ATP-treated conditions is quantified in (**ii**). $N = 4$, Student's *t* test. (**F**) Confocal micrographs (**i**) of control (top panels) or ATP-treated (bottom panels) N2a cells stably expressing Panx1—EGFP immunostained for clathrin heavy chain (Clathrin; red). Panx1—EGFP—clathrin co-distribution in control and ATP-treated conditions is quantified in (**ii**). Scale bars = 10 μm. Inset scale bars = 5 μm. $N = 4$, Student's *t* test. *$P < 0.05$. Hoechst (blue) was used as a nuclear counterstain.

Figure 5. ATP-evoked Panx1 internalization is dynamin-independent. Confocal micrographs of N2a cells stably expressing Panx1—EGFP (green) pretreated with (**A**) vehicle (equivalent volume of DMSO) or (**B**) Dynasore and incubated in 647-transferrin (red) at 4 °C, then fixed and imaged immediately after 4 °C incubation (top panels) or fixed and imaged after stimulation with vehicle (middle panels) or 500 μM ATP (bottom panels) for 30 min at 37 °C. Scale bars = 10 μm. (**C**) Intracellular 647-transferrin in cells pre-incubated with DMSO or Dynasore was quantified relative to 4 °C control. (**D**) Intracellular Panx1 in cells pre-incubated with DMSO or Dynasore was quantified relative to vehicle control. $N = 4$, one-way ANOVA with Dunnett's *post-hoc* test. *$P < 0.05$, **$P < 0.01$.

Figure 6. ATP stimulates increased co-distribution between intracellular Panx1 and markers for the early endosomal and recycling endosomal compartments. (**A**) Panx1—EGFP expression relative to β-actin assessed by Western blotting was unchanged over a 2 h time course in both 500 μM ATP and vehicle control-treated N2a cells stably expressing Panx1—EGFP (**i**, Western blot; **ii**, quantification of three replicates by densitometry). (**B**) Diagram outlining the endosomal system and the antibody markers used (**C** and **D**; Supplemental Figure S3) to demarcate specific compartments therein. Representative confocal micrographs (**i**) of Panx1—EGFP stably-expressed in N2a cells demonstrate Panx1 (green) distribution relative to subcellular markers for the early endosome (**C**; EEA1; red) and recycling endosomes (**D**; Rab14; red) stimulated with ATP (500 μM) for 0.5, 1, and 2 h relative to vehicle control-treated cells (2 h). Panx1 co-distribution with compartment-specific markers was quantified in the central region and peripheral region (**ii**; see 'Materials and Methods'). $N = 4$ per treatment group; central and peripheral regions each analysed independently with one-way ANOVA and Dunnett's *post-hoc*

test. **P* <0.05, ***P* <0.01. (**iii**) Representative STED confocal images of selected regions of interest from coverslips used in (**ii**) obtained using a Leica SP8 STED microscope to confirm localization of Panx1 and EEA1 or Rab14 to common compartments with greater resolution. Scale bars = 10 μm. Inset scale bars = 5 μm. Hoechst (blue) was used as a nuclear counterstain.

Fig. 1 Boyce et al. 2015

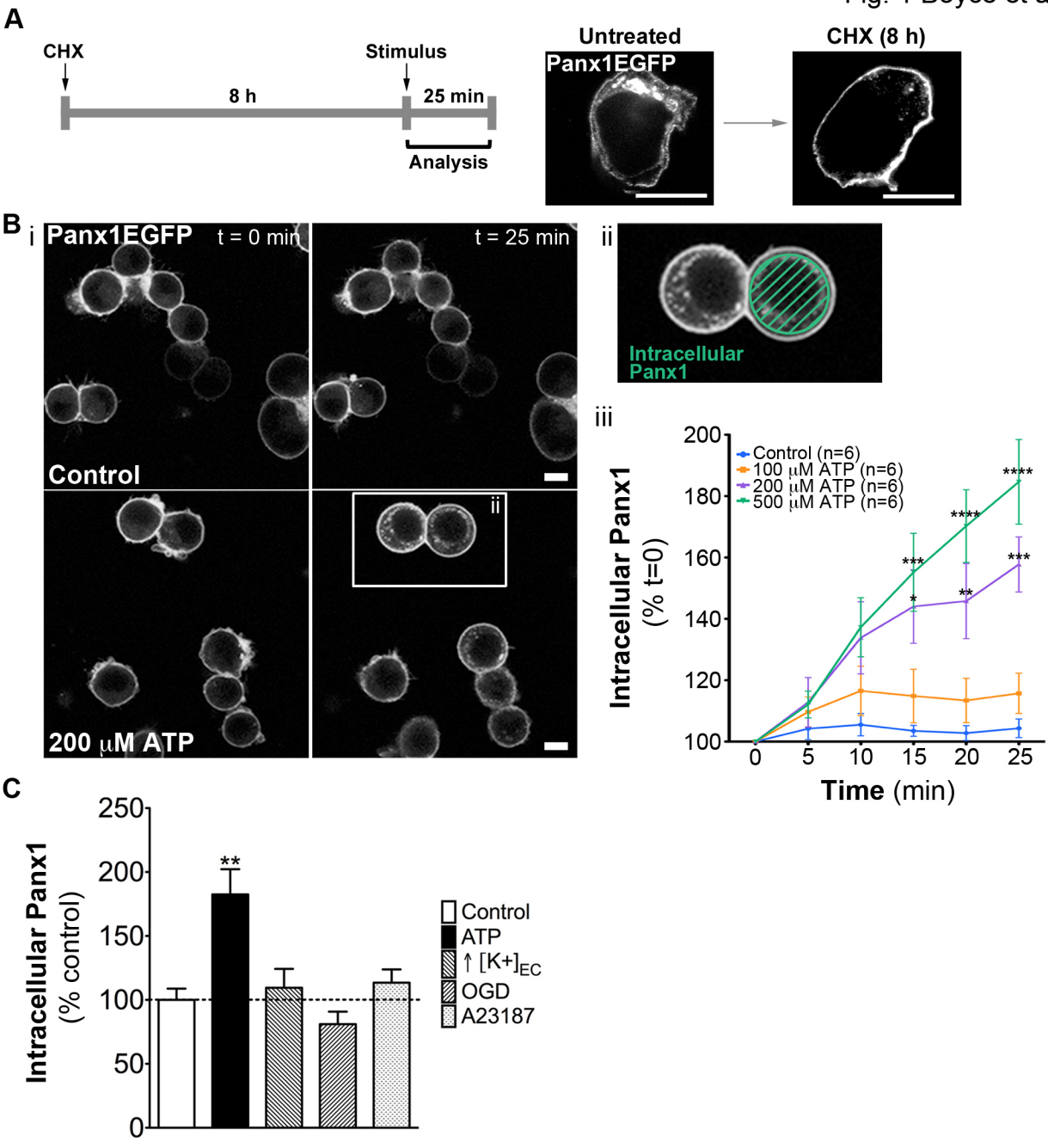

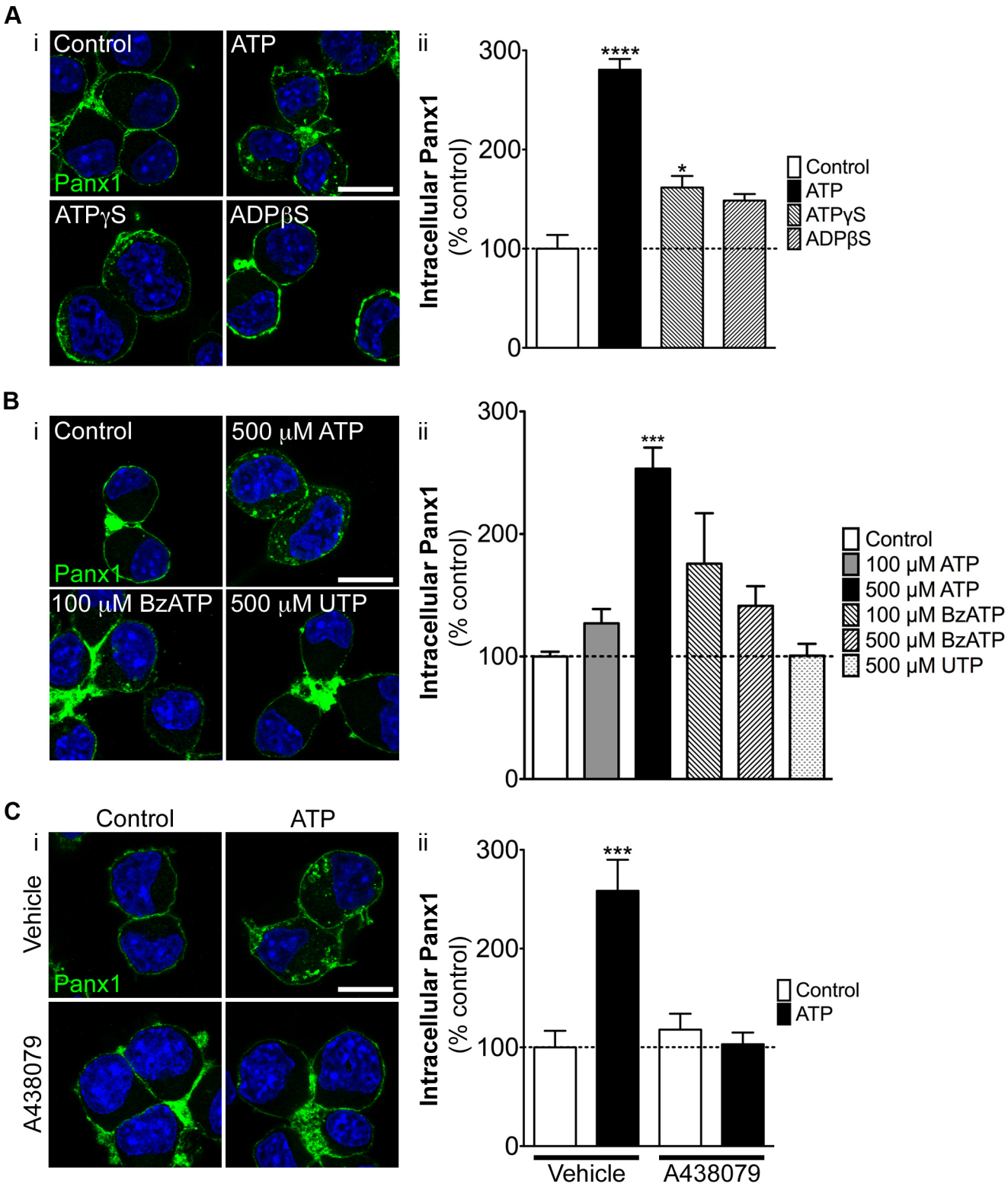
A
i
Control
ATP
Panx1
ATPγS
ADPβS
ii
Intracellular Panx1
(% control)
300
200
100
0
****
*
Control
ATP
ATPγS
ADPβS
B
i
Control
500 μM ATP
Panx1
100 μM BzATP
500 μM UTP
ii
Intracellular Panx1
(% control)
300
200
100
0
***
Control
100 μM ATP
500 μM ATP
100 μM BzATP
500 μM BzATP
500 μM UTP
C
Control
ATP
i
Vehicle
A438079
Panx1
ii
Intracellular Panx1
(% control)
300
200
100
0
***
Control
ATP
Vehicle
A438079

Fig. 3 Boyce et al. 2015

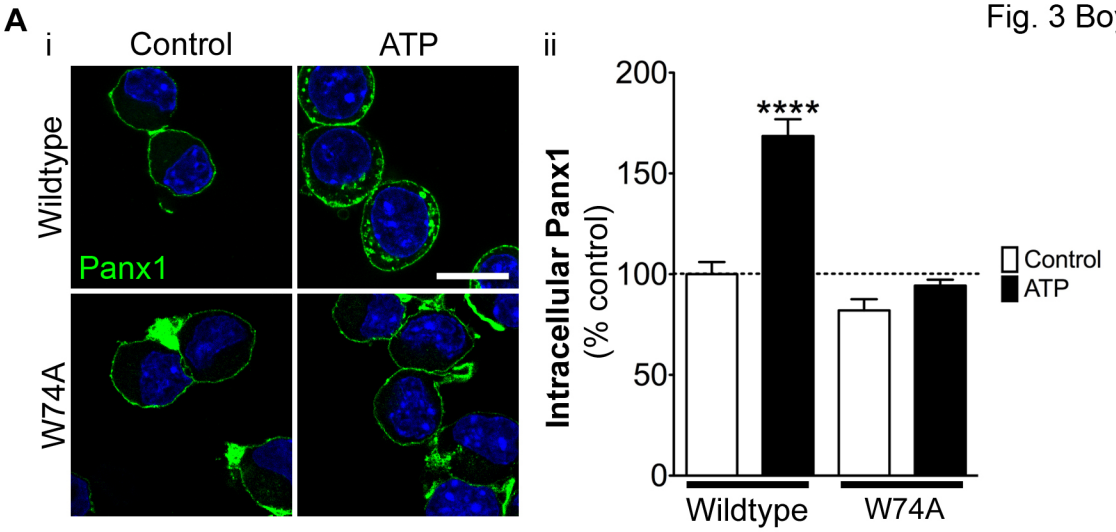

Fig. 4 Boyce et al. 2015

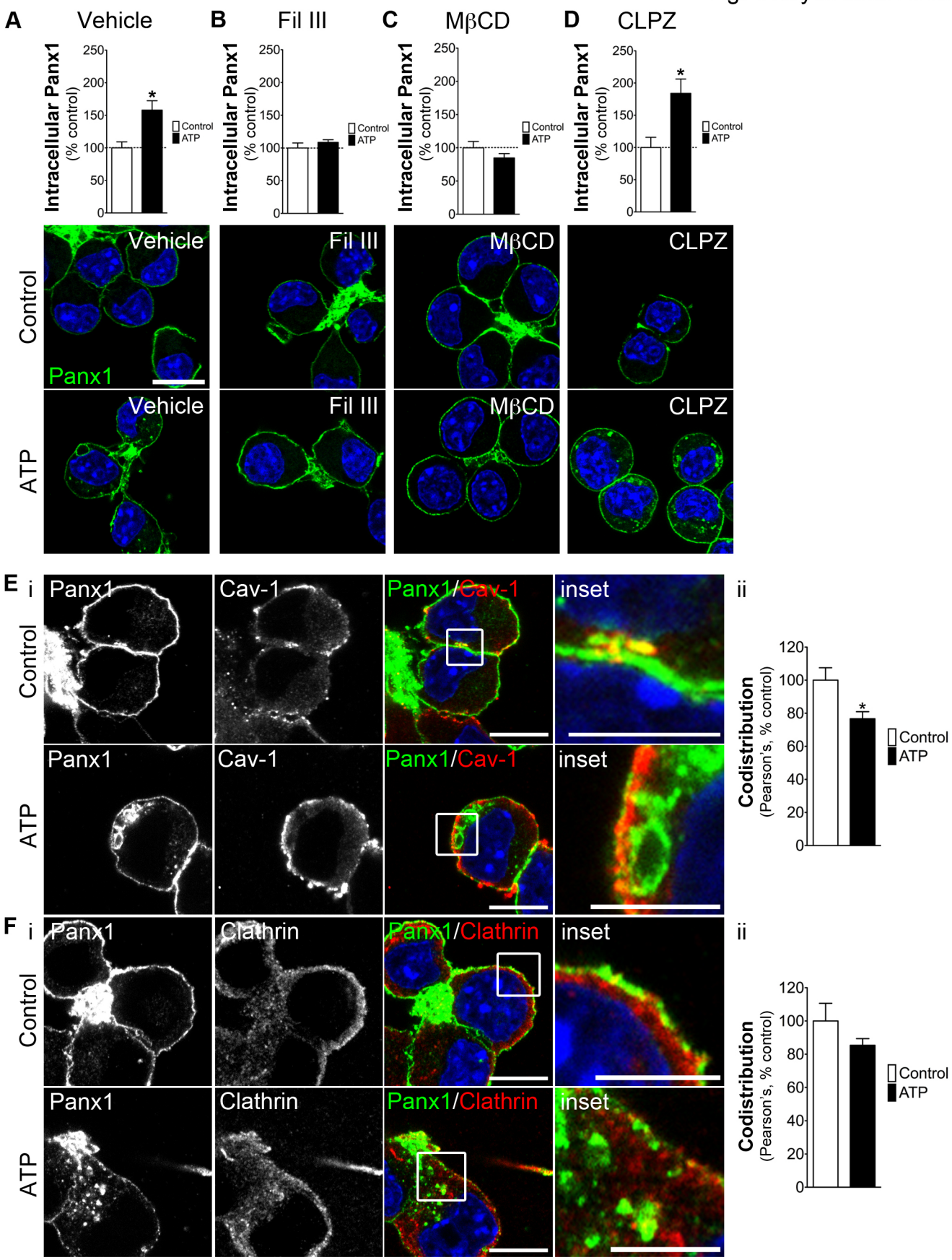

Fig. 5 Boyce et al. 2015

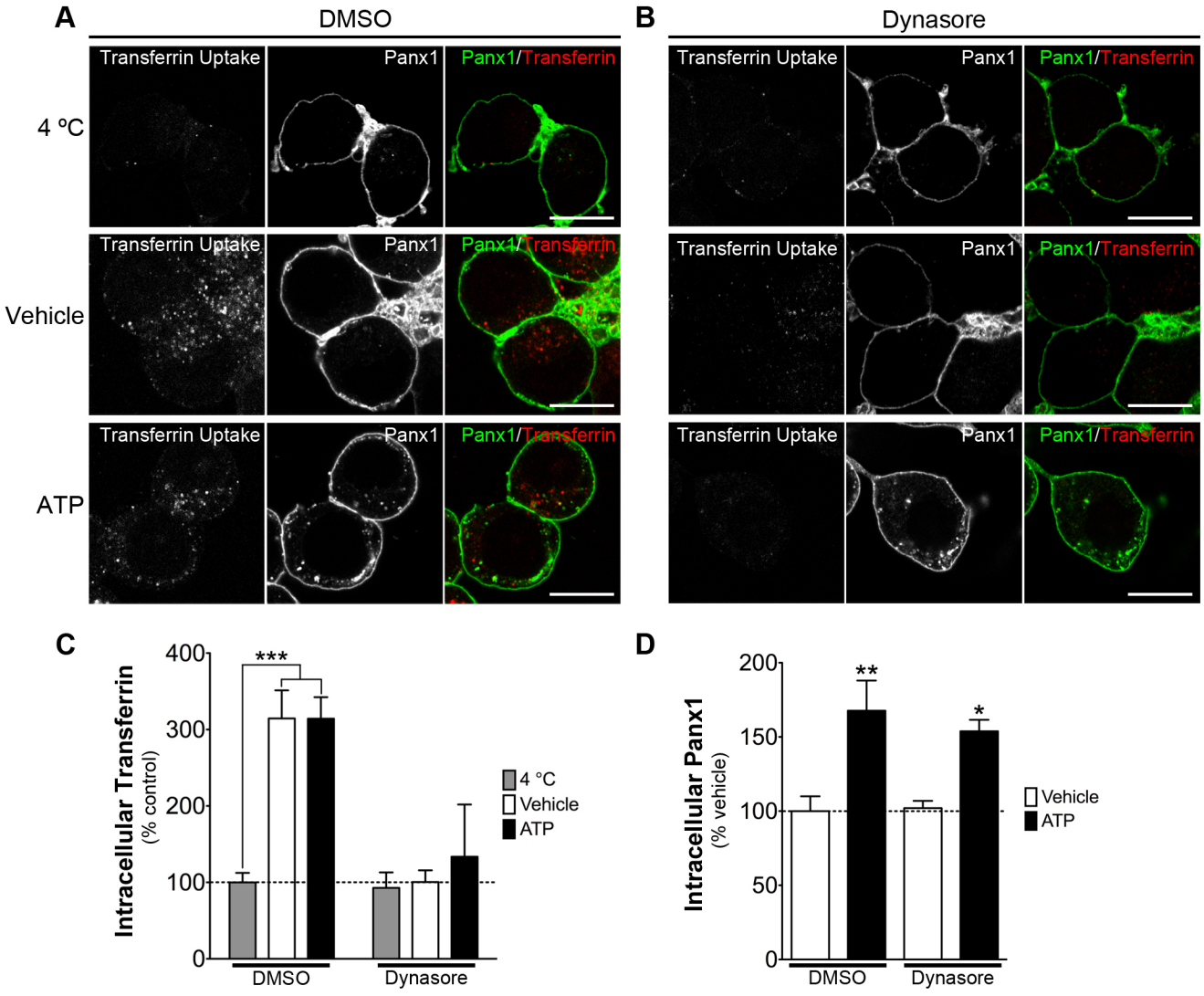

Fig. 6 Boyce et al. 2015

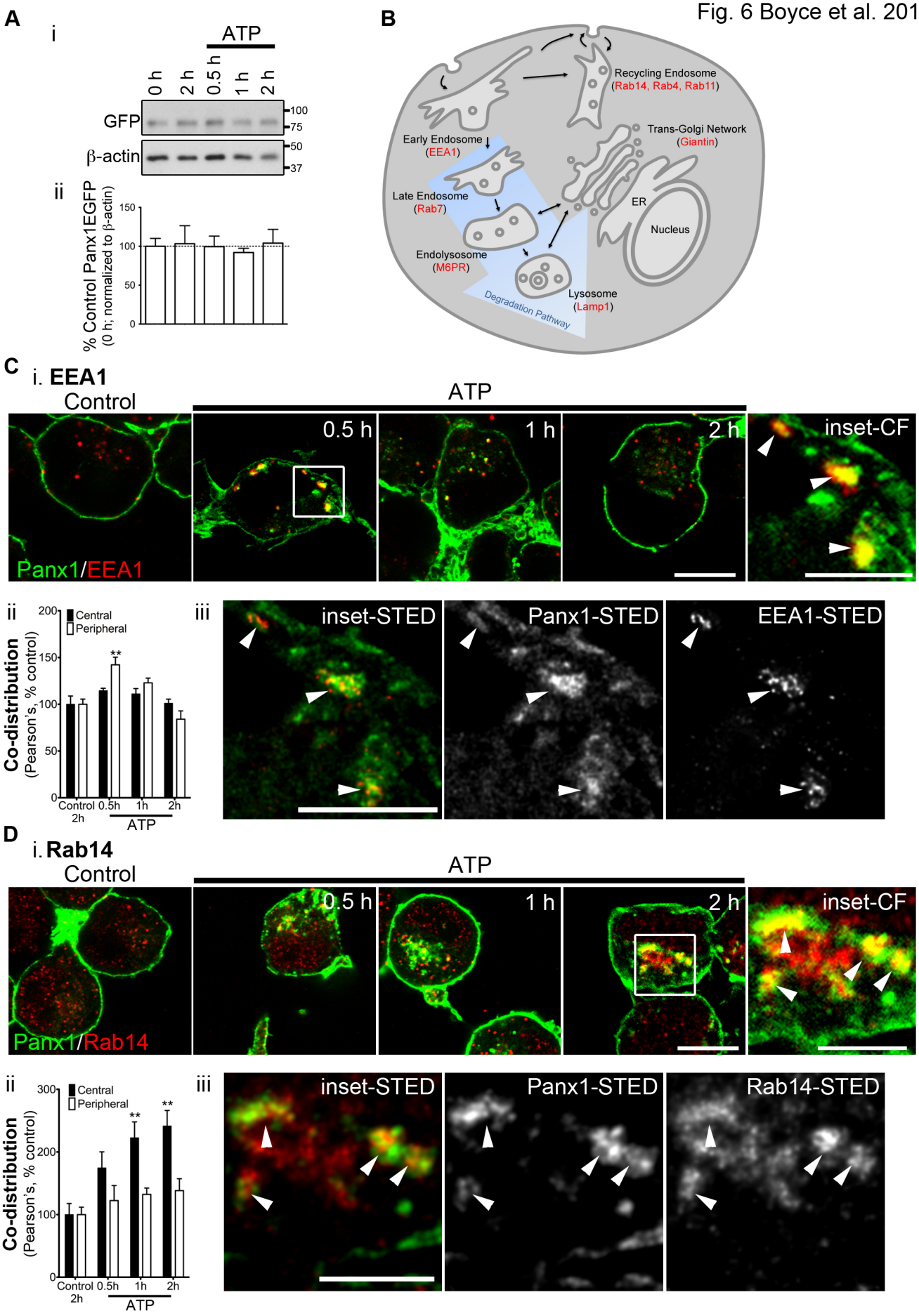

Boyce et al. 2015 Supplemental materials

Supplemental Figure S1. Elevated extracellular ATP diminishes cell surface Panx1. (**A**) Cell-surface luminometry utilizes a primary antibody to an extracellular epitope (Panx1-EL2; **i**) to determine the surface expression in non-permeabilized cells as a percentage of the whole cell expression in permeabilized cells, as depicted in (**ii**). (**iii**) Surface expression of Panx1—EGFP transiently expressed in HEK293T cells is decreased by ATP (200 μM), but not by elevated K^+ concentration (10 mM). $N = 3$, one sample *t* test compared to hypothetical value of 100%. $*P < 0.05$.

Supplemental Figure S2. N2a cells express caveolin-1, but not caveolin-2. Cav-1 mRNA is expressed in both the SVZ and to a lesser degree N2a cells, while Cav-2 is expressed exclusively in the sub-ventricular zone, as demonstrated by RT-PCR. GAPDH was used as a loading control.

Supplemental Figure S3. Subcellular compartments are distinguishable using confocal microscopy and codistribution analysis. Representative confocal micrographs of CHX-treated N2a cells stably expressing Panx1—EGFP indicate limited co-distribution between (**A**) EEA1 (green) and giantin (red) – markers for the early endosome and the Golgi, respectively; minor codistribution between (**B**) EEA1 (green) and Lamp1 (red), markers for the early endosome and lysosome, respectively; and a high degree of co-distribution between (**C**) Rab14 (green) and Rab4 (red) – two markers for recycling endosomal compartments. Scale bars = 10 μm. (**D**) Co-distribution was quantified using Pearson's correlation coefficient. $N = 4$ biological replicates per experimental condition.

Supplemental Figure S4. ATP stimulates reduced codistribution of intracellular Panx1 with components of the degradative pathway and increased co-distribution with components of the recycling endosomal system (**A**) Pearson's correlation coefficients for Panx1—EGFP and the markers for subcellular compartments in N2a cells stably expressing Panx1—EGFP under control conditions (2 h vehicle) in the central and peripheral regions (see 'Materials and Methods'). Representative confocal micrographs (**i**) of N2a cells stably expressing Panx1—EGFP demonstrate Panx1 (green) distribution relative to the endolysosome (**B**; M6PR; red) stimulated with ATP or vehicle control for 2 h, intracellular and submembrane co-distribution quantified in (**ii**). Representative confocal micrographs (**i**) of N2a cells stably expressing Panx1—EGFP demonstrate Panx1 (green) distribution relative to the late endosome (**C**; Rab7; red), lysosome (**D**; Lamp1; red), Golgi (**E**; Giantin; red), or additional recycling endosomes (**F** – Rab11 or **G** – Rab4; red) stimulated with ATP (500 μM) for 0.5, 1, and 2 h relative to vehicle control-treated cells (2 h), central and peripheral co-distribution quantified in (**ii**). Scale bars = 10 μm. Inset scale bars = 5 μm. $N = 4$ per treatment group; central and peripheral each analysed independently with one-way ANOVA with Dunnett's *post-hoc* test. Hoechst (blue) was used as a nuclear counterstain. $*P < 0.05$, $**P < 0.01$, $***P < 0.001$, $****P < 0.0001$.

Supplemental Movie S1. N2a cells stably expressing Panx1—EGFP treated with 500

μM ATP at time zero. Plasma membrane, vesicles, and Golgi are labelled with WGA-TRITC (red). Internalized Panx1—EGFP -positive vesicles appear yellow. Cells were imaged every minute over a 25-minute span. Scale bar = 10 μm.

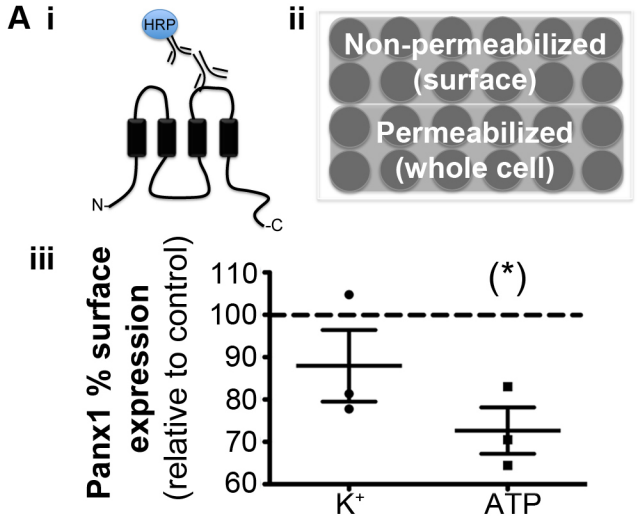
A i
HRP
N
C
ii
Non-permeabilized (surface)
Permeabilized (whole cell)
iii
Panx1 % surface expression (relative to control)
110
100
90
80
70
60
(*)
K+
ATP

Suppl. Fig. 2 Boyce et al. 2015

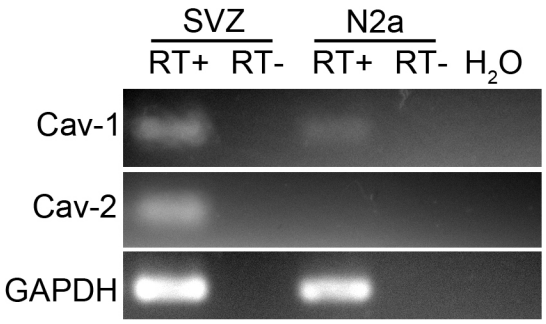

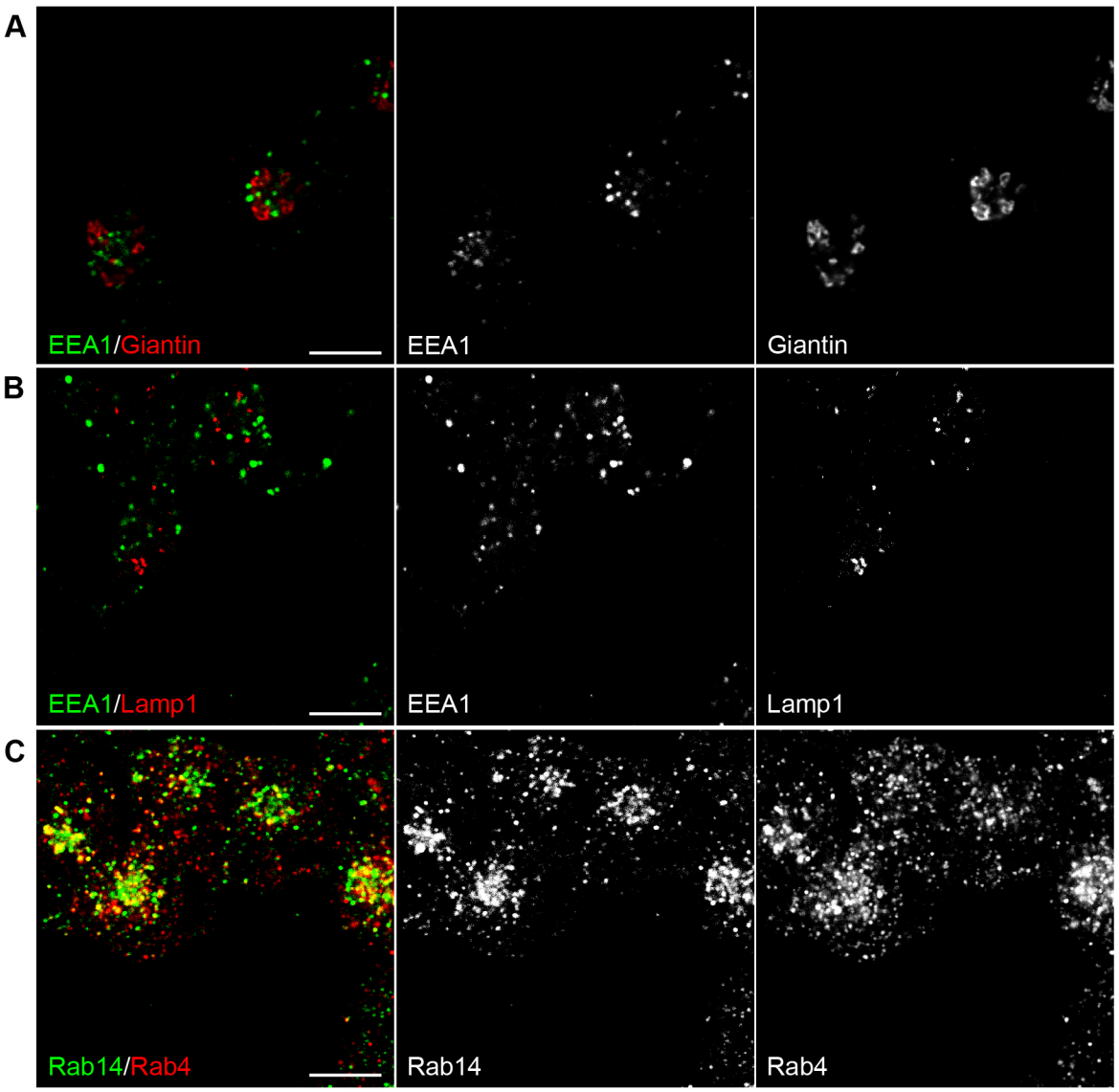
A
EEA1/Giantin
EEA1
Giantin
B
EEA1/Lamp1
EEA1
Lamp1
C
Rab14/Rab4
Rab14
Rab4

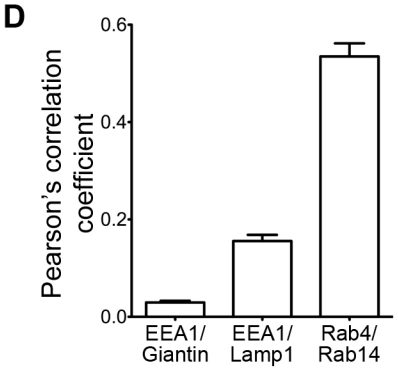
D
Pearson's correlation coefficient
0.6
0.4
0.2
0.0
EEA1/ Giantin
EEA1/ Lamp1
Rab4/ Rab14

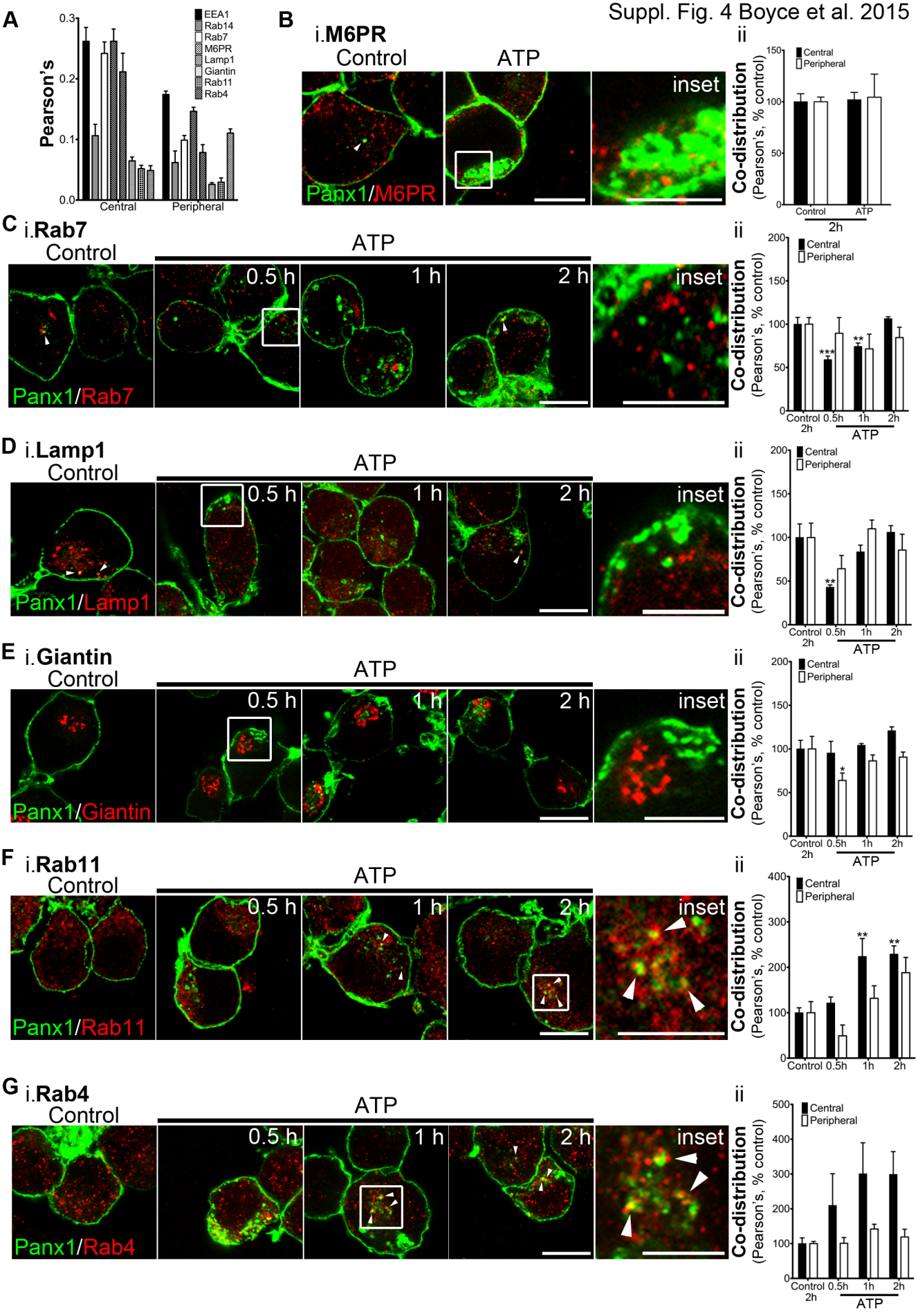
A
Pearson's
EEA1
Rab14
Rab7
M6PR
Lamp1
Giantin
Rab11
Rab4
Central
Peripheral
B
i.M6PR
Control
ATP
inset
Panx1/M6PR
ii
Co-distribution
(Pearson's, % control)
Central
Peripheral
Control
ATP
2h
C
i.Rab7
Control
ATP
0.5 h
1 h
2 h
inset
Panx1/Rab7
ii
Co-distribution
(Pearson's, % control)
Central
Peripheral
Control
0.5h
1h
2h
2h
ATP
D
i.Lamp1
Control
ATP
0.5 h
1 h
2 h
inset
Panx1/Lamp1
ii
Co-distribution
(Pearson's, % control)
Central
Peripheral
Control
0.5h
1h
2h
2h
ATP
E
i.Giantin
Control
ATP
0.5 h
1 h
2 h
inset
Panx1/Giantin
ii
Co-distribution
(Pearson's, % control)
Central
Peripheral
Control
0.5h
1h
2h
2h
ATP
F
i.Rab11
Control
ATP
0.5 h
1 h
2 h
inset
Panx1/Rab11
ii
Co-distribution
(Pearson's, % control)
Central
Peripheral
Control
0.5h
1h
2h
G
i.Rab4
Control
ATP
0.5 h
1 h
2 h
inset
Panx1/Rab4
ii
Co-distribution
(Pearson's, % control)
Central
Peripheral
Control
0.5h
1h
2h
2h
ATP